LETTERS
PUBLISHED ONLINE: 27 MAY 2012 | DOI: 10.1038/NGEO1479
nature geoscience

Landslide erosion coupled to tectonics and river incision

Isaac J. Larsen* and David R. Montgomery

The steep topography of mountain landscapes arises from interactions among tectonic rock uplift, valley incision and landslide erosion on hillslopes. Hillslopes in rapidly uplifting landscapes are thought to respond to river incision into bedrock by steepening to a maximum stable or 'threshold' angle[1–3]. Landslide erosion rates are predicted to increase nonlinearly as hillslope angles approach the threshold angle[1–7]. However, the key tenet of this emerging threshold hillslope model of landscape evolution—the coupled response of landslide erosion to tectonic and fluvial forcing—remains untested. Here we quantify landslide erosion rates in the eastern Himalaya, based on mapping more than 15,000 landslides on satellite images. We show that landslide erosion rates are significantly correlated with exhumation rates and stream power and that small increases in mean hillslope angles beyond 30° translate into large and significant increases in landslide erosion. Extensive landsliding in response to a large outburst flood indicates that lateral river erosion is a key driver of landslide erosion on threshold hillslopes. Our results confirm the existence of threshold hillslopes and demonstrate that an increase in landslide erosion rates, rather than steepened hillslope angles, is the primary mechanism by which steep uplands respond to and balance rapid rates of rock uplift and bedrock river incision in tectonically active mountain belts.

The threshold hillslope paradigm is rooted in the observation that hillslope angles throughout mountainous landscapes tend to be symmetrically distributed about a mean value with a mode comparable to the friction angle of granular material[1,2,8–10]. In contrast to how hillslope angles and erosion rates increase linearly to keep pace with rock uplift in landscapes with low to moderate tectonic forcing[3,5–7,11], at high uplift rates hillslope angles are thought to be limited by material strength[12], so hillslopes will approach the threshold angle and erosion rates will increase nonlinearly such that the relationship between erosion rates and slope angles approaches asymptotic. Vertical river incision into bedrock is thought to over-steepen hillslopes with gradients near the threshold angle, increasing relief until gravitational stress exceeds material strength and bedrock landsliding occurs[1]. Hence landscapes with hillslope gradients near the threshold angle are thought to respond to increases in uplift-driven river incision by increasing landslide erosion rates, rather than by steepening[1,3,5]. Implicit in the threshold hillslope model are the assumptions that landslide erosion rates spatially track rates of river incision and that landslide erosion rates increase nonlinearly as hillslope gradients approach the threshold angle. In steady-state landscapes, the threshold hillslope model also predicts that landslide erosion rates are spatially coupled with exhumation and rock uplift rates. Strong indirect support for threshold hillslopes exists in the form of an independence of hillslope angles on river incision and exhumation rates[1], correlation of landslide density with exhumation and surface uplift rates[9], nonlinear relationships between erosion rates and hillslope angles[3–7,11] and the finding that landslide erosion rates can match high rates of landscape denudation[13]. However, direct coupling of landslide erosion with river incision and exhumation and the nature of the coupling have not been demonstrated.

We tested the threshold hillslope concept in the eastern Himalaya where the Yarlung Tsangpo River cuts through the Namche Barwa–Gyala Peri massif (Fig. 1a). Here the Tsangpo River drops 2 vertical kilometres within the Tsangpo Gorge[14], where close spatial coupling among high topographic relief, high unit stream power[15,16] and young mineral cooling ages[17,18] suggest high rates of erosion are closely linked with crustal deformation, metamorphism and rapid exhumation[19]. Moreover, the thermochronology (Fig. 1b) and stream power data indicate exhumation and river incision within the eastern Himalaya vary spatially by orders of magnitude[16], whereas mean slope angles vary little (Fig. 1c), making the landscape ideal for testing the threshold hillslope model with landslide erosion data. We quantified multi-decadal landslide erosion rates by generating two inventories of landslide areas: an inventory of 15,257 landslides that occurred before 1974 and an inventory of 558 landslides that occurred between 1974 and 2007. We used the spatial distribution of predicted landslide volumes as a proxy for spatially averaged erosion rates and assessed regional ($>10^3$ km^2) and local ($\leq$100 km^2) spatial coupling among landslide erosion, hillslope angles, stream power and exhumation rates to determine whether the eastern Himalaya harbours threshold hillslopes.

The pre-1974 landslide data show that high rates of landslide erosion are spatially focused within a ~2,000 km^2 region of rapid exhumation along the Yarlung Tsangpo and Po Tsangpo rivers (Fig. 1d). The time period over which the pre-1974 landslides occurred is unknown, but 30 yr provides a limiting constraint (see Methods). To account for infrequently occurring large landslides 'missing' from our inventory because of the short temporal scale of observation, we assume the landslides occurred over three decades and integrate landslide magnitude–frequency distributions following the methodology of refs 13 and 20, which yields erosion rates within the zone of high exhumation of 2–6 mm yr^{-1} (see Supplementary Information). Erosion rates outside the zone of high exhumation are 0.3–1.0 mm yr^{-1} and are locally greater where large, isolated landslides occur on glacially steepened valley walls. Comparison of the distributions of local-scale erosion rates indicates that median landslide erosion rates within the high exhumation zone are significantly

Department of Earth and Space Sciences and Quaternary Research Center, University of Washington, Seattle, Washington 98195-1310, USA.
*e-mail: larseni@uw.edu.

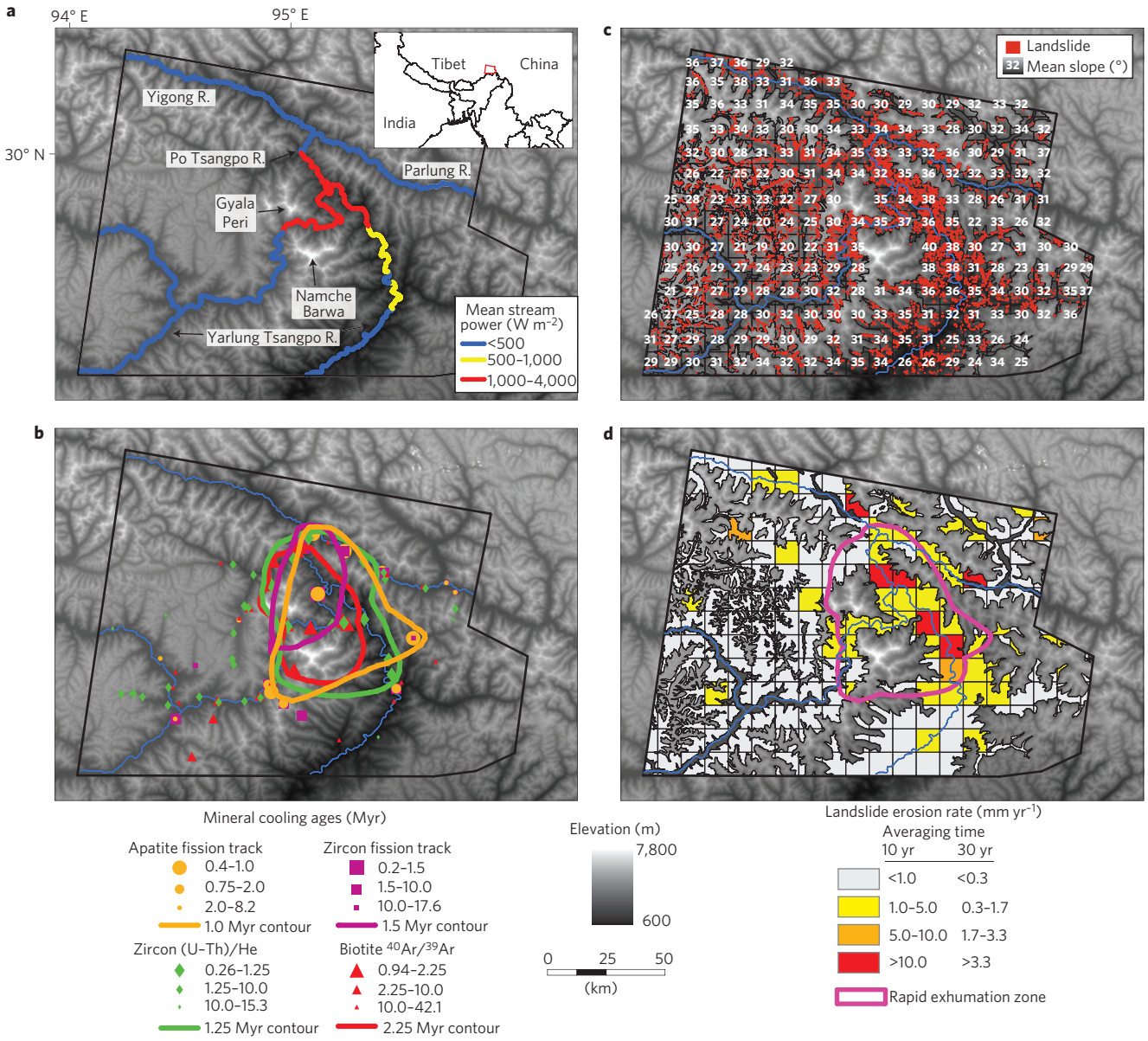

Figure 1 | Spatial patterns of stream power, mineral cooling ages, hillslope angles and pre-1974 landslide erosion rates in the eastern Himalaya. **a**, Stream power[16]. **b**, Mineral cooling ages[16–18]. **c**, Mean hillslope angles. **d**, Pre-1974 landslide erosion rates. The mineral cooling age contours correspond approximately to a 2 mm yr^{-1} exhumation rate and delineate the high versus low exhumation zones (see Methods).

greater by a factor of four than landslide erosion rates outside this region (Fig. 2a).

The 1974–2007 landslide data indicate that the highest landslide erosion rates occur along the Po Tsangpo River downstream from Zhamu Creek (Supplementary Fig. S1), a tributary of the Yigong River, where a large landslide dam[21] breached catastrophically in 2000. The ensuing outburst flood caused extensive landslide erosion; field inspection of sites along the upstream path of the flood indicated the toes of soil-mantled hillslopes were scoured to fresh bedrock, which triggered translational landslides that were identified on satellite images. Landslide erosion rates locally reach 15 mm yr^{-1} for 10-km-long river reaches during the 33-yr period (Fig. 3) and the flood-induced landslides account for ~70% of the landslide erosion in the high exhumation zone (Supplementary Table S1). Landslide erosion rates in the high exhumation region were 4–21 mm yr^{-1} from 1974 to 2007, whereas rates in the low exhumation zone were estimated to be 1–4 mm yr^{-1}. Although the spatial maxima in landslide erosion are similar for both landslide inventories (Fig. 1d and Supplementary Fig. S1), the pre-1974 landslide inventory provides a more representative view of the spatial pattern of landslide erosion because the outburst flood influenced the 1974–2007 erosion pattern.

The large differences in landslide erosion between the high and low exhumation zones exist despite only a 3° difference in the modal hillslope gradient of the two regions (Fig. 2b). Hillslopes in the high exhumation zone have a very limited capacity to steepen in response to rock uplift and river incision, as reflected in the close correspondence between the landslide and landscape-wide slope angle distributions.

The spatial focus of high landslide erosion rates from both landslide inventories corresponds to the high exhumation zone, where mineral cooling ages[16–18] are significantly younger than cooling ages from the surrounding landscape (Supplementary Fig. S2). Hence decadal-scale landslide erosion rates and exhumation rates averaged over 10^5–10^6 yr timescales exhibit a significant degree of

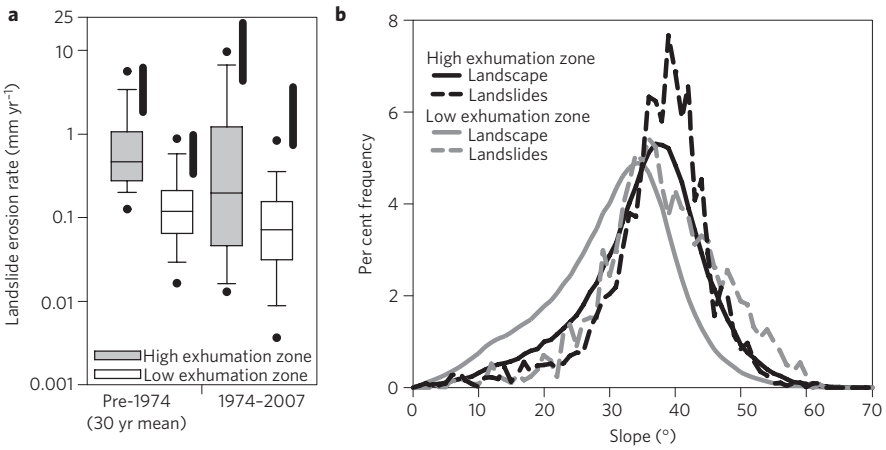

Figure 2 | Landslide erosion rate and hillslope angle distributions for the high and low exhumation zones. a, Distributions of landslide erosion rates from each grid cell are depicted with boxplots; lines to the right of each boxplot show the range of erosion rates estimated by integration of landslide volume–frequency distributions (see Supplementary Information). The boxes span the inter-quartile range, the line denotes the median, whiskers denote 10th and 90th percentiles and circles denote 5th and 95th percentiles. Each pair has significantly different medians ($p \leq 0.001$; see Methods). **b**, Hillslope angle distributions for the high exhumation zone (mode = 37°), 1974–2007 high exhumation zone landslides (mode = 39°), low exhumation zone (mode = 34°) and 1974–2007 low exhumation zone landslides (mode = 36°). The Zhamu Creek landslide accounts for ~65% of the 1974–2007 low exhumation zone landslide slope data. Excluding the Zhamu Creek landslide has a minimal influence of the mode, but reduces the mean slope angle by ~3°.

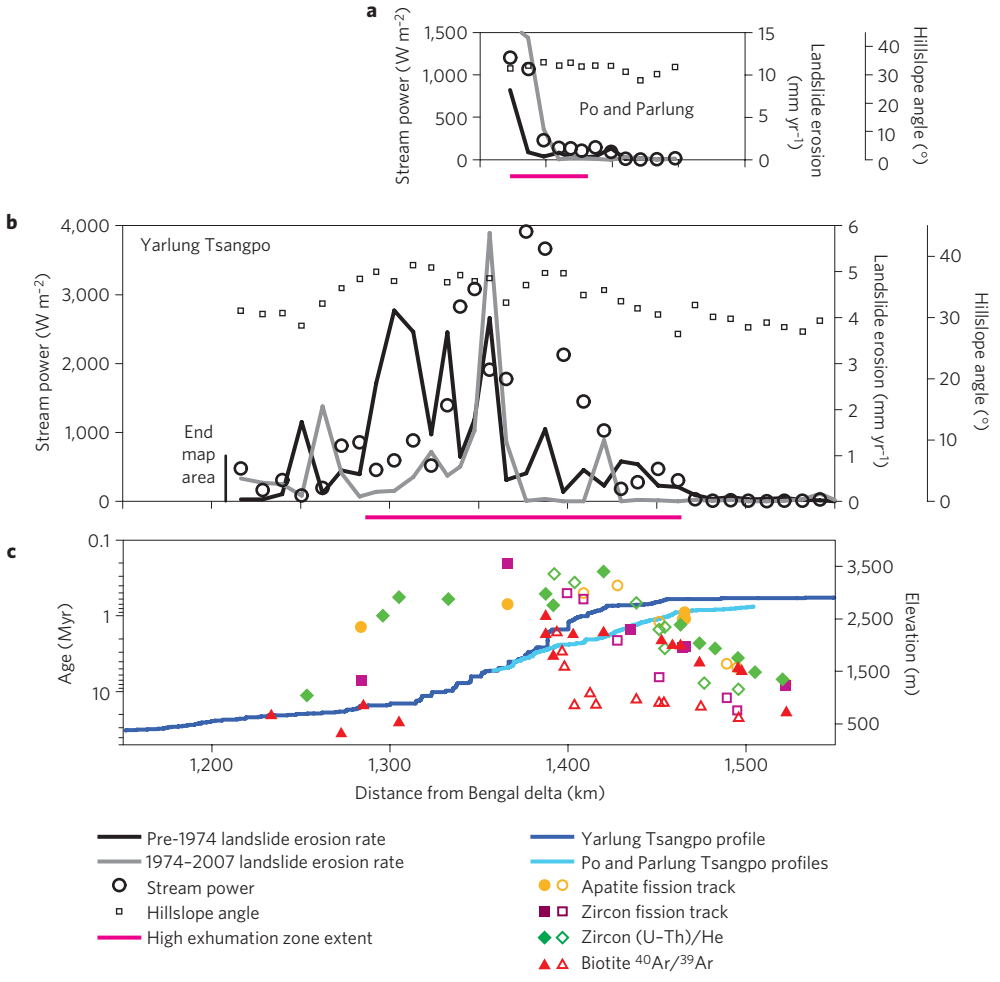

Figure 3 | Patterns of landslide erosion, hillslope angles, stream power and mineral cooling ages along the long profiles of the Yarlung Tsangpo and Po and Parlung Tsangpo rivers. a,**b**, Landslide erosion rate, stream power[16] and hillslope angle for the Po and Parlung Tsangpo rivers (**a**) and Yarlung Tsangpo (**b**). **c**. River long profile and mineral cooling age data[16–18]; filled symbols correspond to the Yarlung Tsangpo and open symbols correspond to the Po and Parlung Tsangpo rivers.

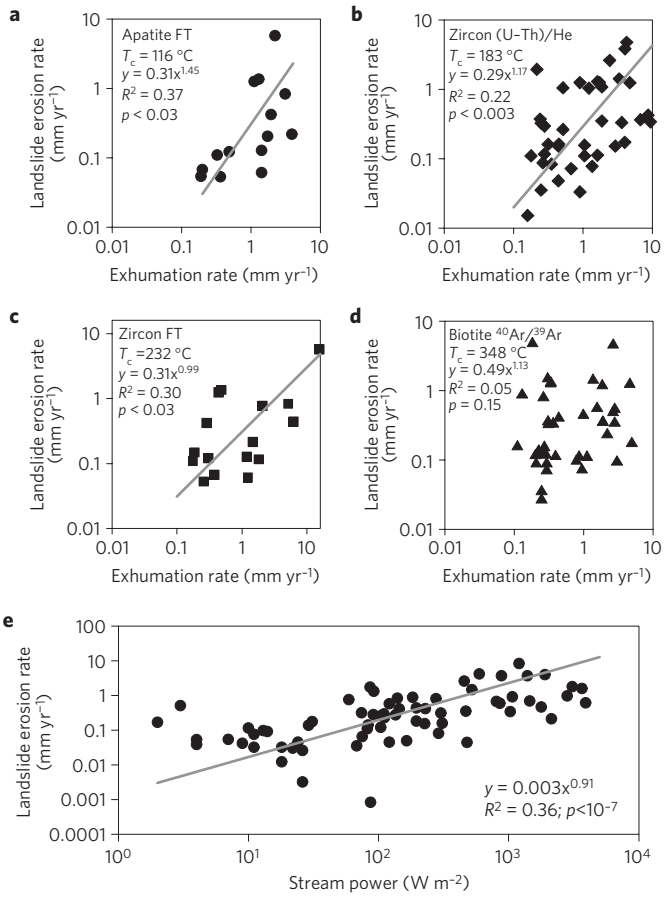

Figure 4 | Landslide erosion rate versus exhumation rate and stream power. a–d, Pre-1974 landslide erosion rates versus exhumation rates for apatite fission track (FT) (**a**), zircon (U–Th)/He (**b**), zircon fission track (**c**) and biotite $^{40}Ar/^{39}Ar$ (**d**) thermochronometers. Closure temperature (T_c) values are from ref. 29. **e**, Pre-1974 landslide erosion rates versus stream power. Lines are shown only for significant regression relationships.

regional-scale spatial coupling. Estimates of exhumation rates in the eastern Himalaya range from 2 to 9 mm yr^{-1} (refs 17,18,22). The multi-decadal landslide erosion rates within the high exhumation zone are of comparable magnitude to long-term exhumation rates, confirming that landslide erosion sustains rapid exhumation in the eastern Himalaya.

Local-scale landslide erosion rates increase weakly, but significantly with increasing exhumation rate for the lower temperature thermochronometers (Fig. 4a–c). The correlation between landslide erosion and exhumation rates generally declines as closure temperatures increase and there is no significant correlation for the highest temperature thermochronometer, biotite $^{40}Ar/^{39}Ar$ (Fig. 4d), indicating a limit to the fidelity at which thermochronometers track modern rates of surface processes, and hence the present topography, as the timescale of exhumation increases. This limiting timescale is approximately the time required to erode through the equivalent of the modern topographic relief, as the biotite $^{40}Ar/^{39}Ar$ closure depth and landscape relief[19] are both of the order of 3.5–7 km in the eastern Himalaya.

The highest landslide erosion rates exhibit a general spatial association with maxima in unit stream power that occur on the Yarlung and Po Tsangpo knickzones (Fig. 3). The landslide data indicate a clear increase in landslide erosion with increasing stream power for the Po Tsangpo and Parlung rivers. Along the Yarlung Tsangpo there is a general trend of increased landslide erosion where stream power is greatest, but individual reaches with high stream power do not always exhibit high landslide erosion rates, which may be due to the relatively short record of landslide occurrence and the stochasticity of landslide-triggering events or potential under-sampling of landslides on the steep hillslopes in this area. However, local-scale landslide erosion rates increase significantly with increasing stream power (Fig. 4e), indicating that stream power and landslide erosion are spatially coupled. The spatial correlation of young mineral cooling ages and high stream power has been cited as strong evidence that river incision drives landscape lowering in the eastern Himalaya and stream power seems to be a reasonable proxy for long-term fluvial incision in this region[16]. The correlation between landslide erosion rates and stream power supports this view, indicating that vertical river incision is a mechanism that drives landslide erosion on threshold hillslopes over long timescales.

Many of the flood-triggered landslides were located on the outside of meander bends (Supplementary Fig. S3), suggesting lateral scour of regolith played an important role in destabilizing hillslopes. As for vertical channel incision, lateral erosion of hillslope toes increases hillslope gradients, causing landslides from hillslopes in the eastern Himalaya that have little capacity to steepen. Hence there are two mechanisms by which river incision drives erosion on threshold hillslopes, the conventional vertical bedrock incision mechanism, and the lateral erosion mechanism demonstrated by the Zhamu Creek outburst flood. The lateral erosion mechanism requires that rates of regolith (soil and fractured rock) production keep pace with landscape lowering, which is a reasonable expectation, given the lack of bedrock outcrops on the hillslopes in the sub-alpine portion of the Tsangpo Gorge, as well as documentation in other rapidly uplifting mountain belts of extensively fractured subsurface bedrock[10] and rapid soil production[23,24]. Furthermore, repeated failure of glacier dams upstream from the Tsangpo Gorge released floods 2–3 orders of magnitude greater than the Zhamu Creek outburst flood[25]. There are hundreds of breached natural dams upstream from the Tsangpo Gorge[26], suggesting that outburst floods occur often enough to allow lateral erosion to be an important mechanism for driving landslide erosion of threshold hillslopes in this region.

Landslide erosion rates are low where mean hillslope angles are less than 30°, but increase nonlinearly where hillslope angles exceed 30° (Fig. 5a), with small increases in hillslope angles leading to large and significant increases in landslide erosion rates (Fig. 5b). This erosion–slope relationship is consistent with previous studies[3–7,11] but demonstrates for the first time that adjustment of landslide erosion rates is the mechanism by which hillslopes with gradients near a strength-limited angle respond to spatially variable exhumation rates, and hence provides critical empirical evidence needed to validate the threshold hillslope model.

The spatial coupling among landslide erosion, stream power and mineral cooling ages indicates a strong link exists among landslide erosion, river incision and exhumation. This link is significant, despite the stochastic nature of landslide-triggering events and the short decadal timescale encompassed by our landslide erosion data. Furthermore, the extensive landslide erosion triggered by the Zhamu Creek outburst flood demonstrates that many hillslopes in the eastern Himalaya are indeed close to the threshold of stability and that lateral erosion by extreme floods is a key mechanism for coupling fluvial and hillslope erosion. The spatial coupling of landslide erosion rates, stream power and exhumation rates confirms that uplands in tectonically active mountain belts balance rapid rates of rock uplift and river incision through adjustment of landslide erosion rates on threshold hillslopes.

Methods

Landslide erosion. The pre-1974 landslide inventory was generated by mapping all landslides visible on ~4-m-pixel-resolution Keyhole-9 Hexagon (KH-9) images. Two KH-9 images, one from 1973 and one from 1975 provide coverage of the entire

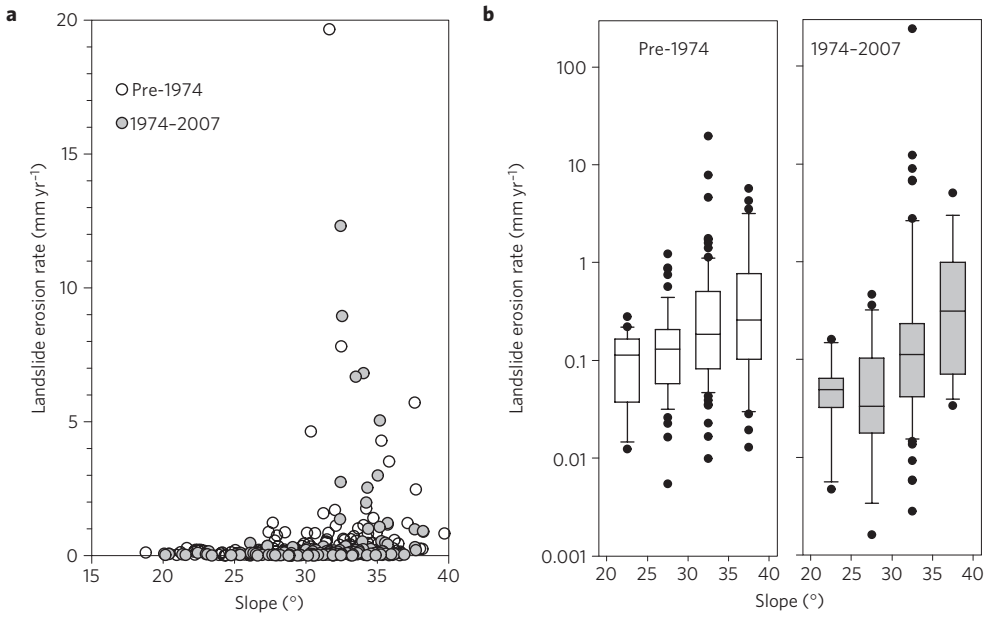

Figure 5 | Landslide erosion rates as a function of hillslope angle. a, Landslide erosion rate versus hillslope angle for the pre-1974 ($n = 201$) and 1974–2007 ($n = 123$) inventories. Data are mean values for individual grid cells. **b**. Distribution of landslide erosion rates as a function of hillslope angle. For both landslide data sets, rates for 20–25° and 25–30° slopes are not significantly different ($p > 0.1$), nor are erosion rates for 30–35° and 35–40° slopes ($p > 0.3$). Erosion rates for 30–35° and 35–40° slopes are significantly greater than rates for 20–25° and 30–35° slopes in both cases ($p < 0.03$). The boxes span the inter-quartile range, the line denotes the median, whiskers denote 10th and 90th percentiles and circles denote outliers. Pre-1974 data average landslide erosion over a 30-yr period. Grid cells with no mapped landslides are not included in the 1974–2007 erosion data, and data for the grid cell with the Zhamu Creek landslide (erosion rate = 241 mm yr^{-1}, slope = 31°) are not shown in **a**.

area (Supplementary Fig. S4); hence we adopt the mean date of 1974 as the date of this inventory. The 1974–2007 landslide inventory was generated by mapping landslides on Landsat (1990, 2000, 2001) and Advanced Spaceborne Thermal Emission and Reflection Radiometer (ASTER; 2001, 2004, 2005, 2007) images, which have a 15-m-pixel resolution, with the exception of the 1990 Landsat image, which has a 30-m-pixel resolution. The 1974–2007 inventory is limited to those landslides that were not present on the 1973/1975 KH-9 images. Landslides were identified on the basis of the distinct spectral signature of soil and rock relative to vegetation; alpine areas above tree line were excluded from the analysis. Landslide scars were mapped and were distinguished from deposits to the extent possible based on downslope changes in the shape and spectral brightness of the disturbed area. Landslide areas were converted to volumes using volume–area scaling relationships. Local-scale erosion rates for each grid cell (see below) were calculated using a volume–area scaling relationship based on 428 measurements of soil and bedrock landslides from the Himalaya[23] (see Supplementary Information for details and erosion rate estimates based on alternative volume–area scaling relationships). Regional-scale landslide erosion rates for the high and low exhumation zone were calculated by means of integration of landslide volume–frequency distributions[20] (see Supplementary Information) and the ranges of values are based on multiple volume–area scaling relationships. The mean depth of material eroded by landslides was determined by summing the landslide volume within each grid cell or region and dividing by the grid cell or region area. The resulting depth of eroded material was converted to an erosion rate by dividing by the time over which the landslides occurred. For the 1974–2007 landslide inventory this was 33 yr, the time between the mean acquisition year of the KH-9 images and the most recent ASTER image. An averaging time of 30 yr was used to assess erosion rates represented by the pre-1974 landslide inventory, which we consider to be a reasonable limiting value for reasons discussed below. The similarity in the power-law portion of the landslide frequency–area distributions for the pre-1974 and 1974–2007 landslide inventories (Supplementary Fig. S5 inset) indicates that these two inventories from different resolution images are drawn from a similar number of landslides[20]. Hence if landslide frequency were similar for the two inventories, landslides in the pre-1974 inventory would have occurred over ~3 decades. Repeat satellite images indicate some landslide scars can revegetate within a decade (Supplementary Fig. S3), suggesting a shorter averaging time and hence higher erosion rates. As a result of uncertainty in the time over which the pre-1974 landslides occurred, we present erosion rates based on the range of averaging times of 10–30 yr (Fig. 1d). As vegetation, cloud cover, topographic shading and other factors can limit landslide detection, we consider the landslide erosion rates for both inventories to be minimum values.

Hillslope angles, stream power and mineral cooling ages. The landscape was divided into 10 km × 10 km grid cells that were clipped to remove areas above tree line and floodplains. Hillslope angles were extracted from the 3 arc-second Shuttle Radar Topography Mission (SRTM) digital elevation model (DEM) with data gaps filled using topographic line data from www.viewfinderpanoramas.org. The clipped 3 arc-second data were used to generate hillslope angle distributions for the high and low exhumation zones and for landslides in the 1974–2007 inventory (hillslope angle distributions were not extracted for the pre-1974 landslide inventory because parallax caused by high topographic relief led to small georeferencing errors and hence misalignment of the KH-9 images and DEM). Slope values averaged over each clipped grid cell were used to assess the relationship between landslide erosion rate and slope in Fig. 5. In addition to alpine areas and floodplains, the bottoms of small valleys were excluded from mean slope calculations by generating a stream network with a threshold contributing area of 8.1 km^2 with streams that terminated in low-gradient valley heads. Areas within 100 m of the streams were excluded from slope calculations. Mean hillslope gradients for areas within 5 km of either side of the channels were projected onto the river long profile after calculating the mean angle for hillslopes adjacent to each segment. Unit stream power data are primarily from ref. 16 but were augmented with values modelled for 10-km-long stream segments following ref. 27 by routing Tropical Rainfall Measuring Mission rainfall estimates from ref. 28 through the World Wildlife Fund-U.S. Geological Survey hydrologically conditioned SRTM DEM. Landslides ≤5 km from rivers were used to calculate erosion rates for 10-km-long stream segments. Mineral cooling data from refs 16 to 18 were used to delineate cooling age contours. The cooling age contours approximately delineate an exhumation rate of ~2 mm yr^{-1}. The fault-bounded core of the Namche Barwa–Gyala Peri antiform has been exhumed at a rate of at least 2 mm yr^{-1} for the past 2.5 Myr, whereas exhumation rates outside the core are an order of magnitude lower[17]; hence the 2 mm yr^{-1} contour provides an independent threshold for delineating the high and low exhumation zones and for comparing spatial patterns in landslide erosion, stream power and topographic data. Exhumation rates were calculated using assumptions similar to those in ref. 18, using closure temperature data from ref. 29 and geothermal gradient information from ref. 30. The zone of rapid exhumation is based on the maximum aerial extent of the ~2 mm yr^{-1} contour for the different thermochronometers. Mineral cooling ages from samples ≤5 km from either side of rivers were projected onto the long profiles in Fig. 3. Landslide erosion data in Fig. 4 are based on summing landslide volumes within a 10-km-diameter circle centred on each thermochronology sample after clipping the circle to the mappable area. Data were excluded if the clipped area was <10% of the original, unclipped area. Exhumation rates in Fig. 4a–d are based on a 75 °C km^{-1} geothermal gradient, the midpoint of the 50–100 °C km^{-1} range[18,30].

Statistical analyses. Hillslope angle modes were determined from 1° slope bins. We tested for significant differences ($p \leq 0.05$) in mineral cooling ages, stream power and landslide erosion inside versus outside the zone of high exhumation

using Mann–Whitney *U* tests, as these data were not normally distributed. Hillslope angle data were normally distributed and differences were assessed using a *t*-test. Differences in landslide erosion as a function of hillslope angle were assessed by binning erosion data in 5° increments. A natural log transformation was applied to the landslide erosion data so they approximated a normal distribution and an analysis of variance with a *post hoc* Fisher's least significant difference test was used to test for differences in erosion rate across the slope groups. Data from grid cells with drainage areas $<1\ km^2$ were not used in statistical analysis of erosion or hillslope angle data. Owing to the coarse resolution of the ASTER and Landsat images, 100 of the 223 grid cells in the 1974–2007 inventory had no mapped landslides; we considered these grid cells to have 'no data' and excluded them from the statistical analysis of the 1974–2007 landslide data. Reduced major axis regression was used to assess the relationship between erosion rates and exhumation rates and erosion rates and stream power. The pre-1974 landslide erosion data were used for regression analyses because the spatial pattern was not influenced by the Zhamu Creek outburst flood.

Received 24 August 2011; accepted 18 April 2012; published online 27 May 2012

References

1. Burbank, D. W. *et al.* Bedrock incision, rock uplift and threshold hillslopes in the northwestern Himalayas. *Nature* **379,** 505–510 (1996).
2. Montgomery, D. R. Slope distributions, threshold hillslopes, and steady-state topography. *Am. J. Sci.* **301,** 432–454 (2001).
3. Montgomery, D. R. & Brandon, M. T. Topographic controls on erosion rates in tectonically active mountain ranges. *Earth Planet. Sc. Lett.* **201,** 481–489 (2002).
4. Roering, J. J., Kirchner, J. W. & Dietrich, W. E. Evidence for nonlinear, diffusive sediment transport on hillslopes and implications for landscape morphology. *Water Resour. Res.* **35,** 853–870 (1999).
5. Binnie, S. A., Phillips, W. M., Summerfield, M. A. & Fifield, L. K. Tectonic uplift, threshold hillslopes, and denudation rates in a developing mountain range. *Geology* **35,** 743–746 (2007).
6. Ouimet, W. B., Whipple, K. X. & Granger, D. E. Beyond threshold hillslopes: Channel adjustment to base-level fall in tectonically active mountain ranges. *Geology* **37,** 579–582 (2009).
7. DiBiase, R. A., Whipple, K. X., Heimsath, A. M. & Ouimet, W. B. Landscape form and millennial erosion rates in the San Gabriel Mountains, CA. *Earth. Planet. Sci. Lett.* **289,** 134–144 (2009).
8. Strahler, A. N. Equilibrium theory of erosional slopes approached by frequency distribution analysis; Part 1. *Am. J. Sci.* **248,** 673–696 (1950).
9. Korup, O. Rock type leaves topographic signature in landslide-dominated mountain ranges. *Geophys. Res. Lett.* **35,** L11402 (2008).
10. Clarke, B. A. & Burbank, D. W. Bedrock fracturing, threshold hillslopes, and limits to the magnitude of bedrock landslides. *Earth. Planet. Sci. Lett.* **297,** 577–586 (2010).
11. Safran, E. B. *et al.* Erosion rates driven by channel network incision in the Bolivian Andes. *Earth Surf. Process. Landf.* **30,** 1007–1024 (2005).
12. Schmidt, K. M. & Montgomery, D. R. Limits to relief. *Science* **270,** 617–620 (1995).
13. Hovius, N., Stark, C. P. & Allen, P. A. Sediment flux from a mountain belt derived by landslide mapping. *Geology* **25,** 231–234 (1997).
14. Brookfield, M. E. The evolution of the great river systems of southern Asia during the Cenozoic India-Asia collision: Rivers draining southwards. *Geomorphology* **22,** 285–312 (1998).
15. Finlayson, D. P., Montgomery, D. R. & Hallet, B. Spatial coincidence of erosional and metamorphic hot spots in the Himalaya. *Geology* **30,** 219–222 (2002).
16. Finnegan, N. J. *et al.* Coupling of rock uplift and river incision in the Namche Barwa-Gyala Peri massif, Tibet. *Geol. Soc. Am. Bull.* **120,** 142–155 (2008).
17. Seward, D. & Burg, J. P. Growth of the Namche Barwa syntaxis and associated evolution of the Tsangpo Gorge: Constraints from structural and thermochronological data. *Tectonophysics* **451,** 282–289 (2008).
18. Stewart, R. J. *et al.* Brahmaputra sediment flux dominated by highly localized rapid erosion from the easternmost Himalaya. *Geology* **36,** 711–714 (2008).
19. Zeitler, P. K. *et al.* Erosion, Himalayan geodynamics, and the geomorphology of metamorphism. *GSA Today* **11,** 4–9 (2001).
20. Malamud, B. D., Turcotte, D. L., Guzzetti, F. & Reichenbach, P. Landslide inventories and their statistical properties. *Earth Surf. Process. Landf.* **29,** 687–711 (2004).
21. Shang, Y. *et al.* A super-large landslide in Tibet in 2000: Background, occurrence, disaster, and origin. *Geomorphology* **54,** 225–243 (2003).
22. Enkelmann, E., Ehlers, T. A., Zeitler, P. K. & Hallet, B. Denudation of the Namche Barwa antiform, eastern Himalaya. *Earth. Planet. Sci. Lett.* **307,** 323–333 (2011).
23. Larsen, I. J., Montgomery, D. M. & Korup, O. Landslide erosion controlled by hillslope material. *Nature Geosci.* **3,** 247–251 (2010).
24. Heimsath, A. M., DiBiase, R. A. & Whipple, K. X. Soil production limits and the transition to bedrock-dominated landscapes. *Nature Geosci.* **5,** 210–214.
25. Montgomery, D. R. *et al.* Evidence for Holocene megafloods down the Tsangpo River gorge, southeastern Tibet. *Quaternary Res.* **62,** 201–207 (2004).
26. Korup, O. & Montgomery, D. R. Tibetan plateau river incision inhibited by glacial stabilization of the Tsangpo gorge. *Nature* **455,** 786–789 (2008).
27. Finnegan, N. J., Roe, G., Montgomery, D. R. & Hallet, B. Controls on the channel width of rivers: Implications for modeling fluvial incision of bedrock. *Geology* **33,** 229–232 (2005).
28. Anders, A. M. *et al.* Spatial patterns of precipitation and topography in the Himalaya. *GSA Spec. Pap.* **398,** 39–54 (2006).
29. Reiners, P. W. & Brandon, M. T. Using thermochronology to understand orogenic erosion. *Annu. Rev. Earth Planet. Sci.* **34,** 419–466 (2006).
30. Craw, D., Koons, P. O., Zeitler, P. K. & Kidd, W. S. F. Fluid evolution and thermal structure in the rapidly exhuming gneiss complex of Namche Barwa-Gyala Peri, eastern Himalayan syntaxis. *J. Metamorph. Geol.* **23,** 829–845 (2005).

Acknowledgements

We thank B. Hallet for stimulating conversations and the Quaternary Research Center for support. I.J.L. thanks the Washington NASA Space Grant fellowship programme, NASA Earth and Space Science Fellowship programme, Geological Society of America (GSA) and GSA Quaternary Geology and Geomorphology Division, Sigma Xi and the University of Washington Department of Earth and Space Sciences for support, H. Greenberg for geographic information system support and J. R. Davis for assistance with curve fitting. Gap-filled DEM data were provided courtesy of www.viewfinderpanoramas.org.

Author contributions

I.J.L. and D.R.M. jointly designed the study and wrote the manuscript. I.J.L. conducted landslide mapping and data analysis.

Additional information

The authors declare no competing financial interests. Supplementary information accompanies this paper on www.nature.com/naturegeoscience. Reprints and permissions information is available online at www.nature.com/reprints. Correspondence and requests for materials should be addressed to I.J.L.